Contents lists available at ScienceDirect

Diamond & Related Materials

journal homepage: www.elsevier.com

Carbon nanotubes synthesis using siliceous breccia as a catalyst source

Arun Kumar [a], Yulia Kostikov [b], Marco Zanatta [a], Gian Domenico Sorarù [c], Beate Orberger [d, e], Gilbert Daniel Nessim [b], Gino Mariotto [a, *]

[a] Department of Computer Science, University of Verona, 37134 Verona, Italy
[b] Department of Chemistry & Bar Ilan Institute for Nanotechnology and Advanced Materials (BINA), Bar Ilan University, Ramat Gan, 52900, Israel Bar Ilan University, Ramat Gan 52900, Israel
[c] Department of Industrial Engineering, University of Trento, 38123 Trento, Italy
[d] ERAMET RESEARCH SLN, 1 Avenue Albert Einstein, 78190 Trappes, France
[e] GEOPS, Université Paris Saclay, Bât 504, 91405 Orsay Cedex, France

ARTICLE INFO

Keywords:
Carbon nanotubes
Chemical vapor deposition
Siliceous breccia
Fe catalyst
Iron oxyhydroxides

ABSTRACT

In this work, siliceous breccia, a natural rock powder composed essentially of SiO_2 α-quartz, has been employed directly as a catalyst without any chemical treatment for the synthesis of carbon nanotubes (CNTs) via chemical vapor deposition (CVD). In addition to quartz, it contains dispersed micro-inclusions of iron oxide-hydroxides, goethite or hematite, which act as catalysts to dissociate the hydrocarbon precursors and form carbon nanostructures. The catalytic performance of this powder was evaluated for C_2H_4 decomposition at 750 °C, with and without H_2 flux. Thermal oxidation stability and carbon yield were measured by means of thermogravimetric analysis. Structural and vibrational characterization of the resulting material was carried out by environmental scanning electron microscopy (ESEM) and micro Raman spectroscopy. ESEM images show that the H_2 addition affects the CNT diameter. We observed that the addition of H_2 to the C_2H_4 flux effectively removes amorphous carbon leading to taller growth of nanotubes. This concept provides a highly economical way for large-scale synthesis of CNTs.

1. Introduction

In the past two decades, carbon nanotubes (CNTs) have been the target of extensive investigations due to their unique/unparalleled physicochemical properties [1,2] and their potential applications in the field of nanoscience and nanotechnology. Examples include electronics [3–5], high-strength polymer composites [6,7], nanoprobes in high-resolution imaging [8], and hydrogen storage [9]. This technological relevance gave rise to an intense research activity on catalytic chemical vapor deposition (CVD), which has been extensively considered for large-scale synthesis of CNTs [10,11] from the decomposition of various hydrocarbons using transition metals as catalysts on different metal oxides supports [12]. Unfortunately, large-scale production of CNTs via catalytic CVD is still expensive. In fact, in addition to the availability of the carbon source, the main cost factors derived from the preparation of substrates (e.g. silicate, aluminates) as well as from the finely dispersed diffusion of metal particles (e.g. Fe, Ni, Mg) on them. However, these transition metals and their oxides can be easily found inside many natural materials, such as rocks and minerals. Consequently, the question arises as to whether CNTs can grow on such minerals by the pyrolysis of hydrocarbon gases at the laboratory level and later on an industrial scale at a reasonable cost. In order to produce CNTs so far, several natural materials such as clay minerals have been tested as carriers of catalytically active metals (e.g., smectite [13], montmorillonite, zeolites [14], sepiolite, kaolinite, nontronite [15], and natural lava [16–18], forsterite, diopside, quartz, magnesite and brucite [19]. In the reported references also, the preparation of the metal-based catalyst is carried out before the growth process by various chemical routes such as ion-exchange reaction in water solutions of respective salts, wet-chemical preparation, or suspension by stirring and then separation of metal particles. Thus, the catalyst preparation is still involved in depositing Fe ions onto the clay matrix. Actually, the Fe ions originally in the minerals can be directly used to catalyse the growth of nanocarbons.

With this concern, we have to mention that there have been reports in the literature where Fe/SiO_2 is not considered as the best catalyst/support combination for CNT production [20,21]. Moreover, Lee et al. [22] investigated the effect of Ni, Fe and Co catalysts using silica as

* Corresponding author.
Email address: gino.mariotto@univr.it (G. Mariotto)

https://doi.org/10.1016/j.diamond.2019.05.018
Received 5 March 2019; Received in revised form 14 May 2019; Accepted 23 May 2019
Available online xxx
0925-9635/

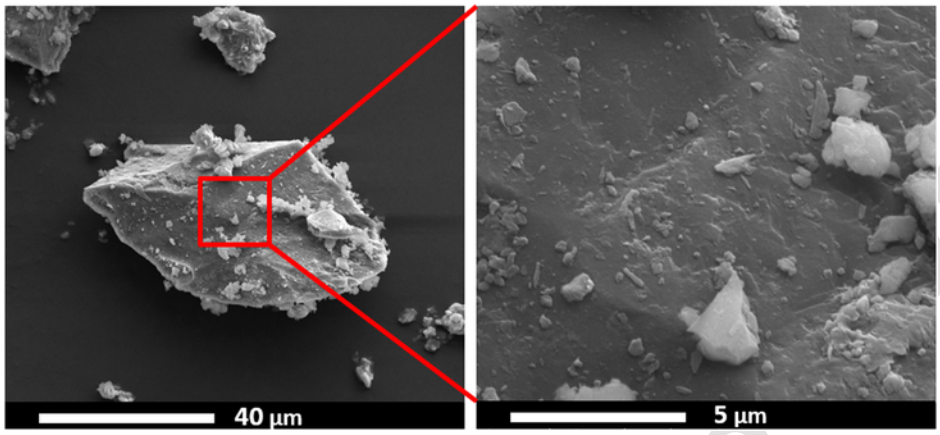

Fig. 1. ESEM image of the siliceous breccia powder.

Table 1
Elemental composition of the natural siliceous breccia powder used in this study as obtained by EDX microanalysis.

Elements	Si	O	Fe	Mg
(wt%)	53.26	45.59	0.39	0.75
(at%)	39.64	59.57	0.15	0.65

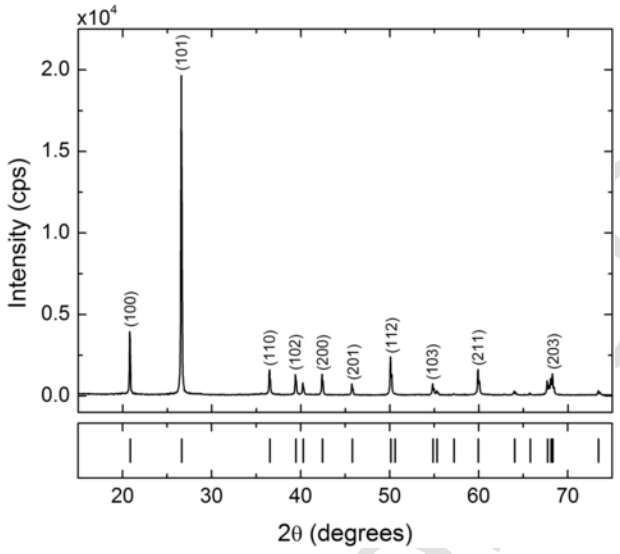

Fig. 2. Typical experimental XRD pattern measured on the siliceous breccia powder. The XRD pattern corresponds to the SiO_2 α-quartz. The calculated Bragg peak positions for α-quartz are shown in the lower panel. The Miller indexes of the main reflections are also reported.

support material for the CNTs synthesis: they found that CNTs growth rate increased according to the following sequence: Fe, Co, Ni. In spite of this, Fe catalyst resulted in the best crystallinity of the synthesized CNTs [22]. This finding supports the hypothesis advanced by Inoue et al. [23], that the role of support can be considered non-primary if the catalytic particle size is in the range between micrometer and tens of nanometers. However, in the case of SWCNTs growth where the catalytic particle size is of few nanometers scale, the role of support cannot be neglected [23]. Recently we were successful in synthesizing CNTs starting from laterite mineral using a CVD reactor operated between 700 and 900 °C [24]. Despite a huge progress in CNT research over the years, we are still in process to fabricate well-defined tailored

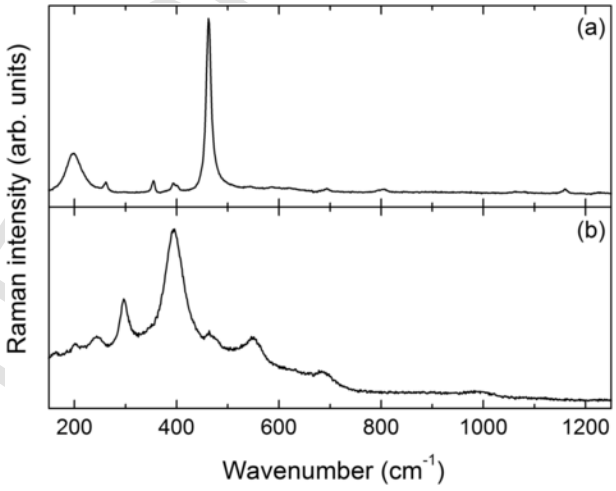

Fig. 3. Typical experimental Raman spectra obtained on the siliceous breccia starting powder showing the two phases detected: (a) α-quartz, as paramount component and (b) goethite in form of micro-inclusions.

CNTs in large quantities using a cost-effective CVD technique [25,26]. In fact, regarding the CVD synthesis, it is generally acknowledged that the type of carbon source and the carrier gas influences the quantity and quality of synthesized CNTs [27,28]. While, the studies regarding the influence of the H_2 gas in growth process as well as its effect on CNTs morphology have been thoroughly investigated [27–30].

The present study examines the possibility of using natural siliceous breccia (SB) [31] as a catalyst source for CNT synthesis. To our knowledge, the growth of CNTs on this kind of catalyst source has not yet been reported. In particular, siliceous breccia in form of powder has been used as a catalyst source for the CNTs growth, which was achieved via CVD underflow of proper C_2H_4 and H_2 mixtures. In fact, by varying the C_2H_4/H_2 ratio it is possible to modulate the rate of atomic carbon deposition, reduce the amorphous carbon formation, and finally tune the size of the synthesized CNT [27,29,30]. The carbon yield, as determined by thermogravimetric analysis, was measured to be about 27% and 43% for CNTs synthesized with and without H_2 flux, respectively. The structural/microstructural characteristics and vibrational properties of the pristine powder and of the as-grown CNTs have also been explored in detail using either ESEM or micro-Raman spectroscopy. The obtained results suggest that siliceous breccia powder is a promising candidate towards an effective and low-cost mass production of the CNTs.

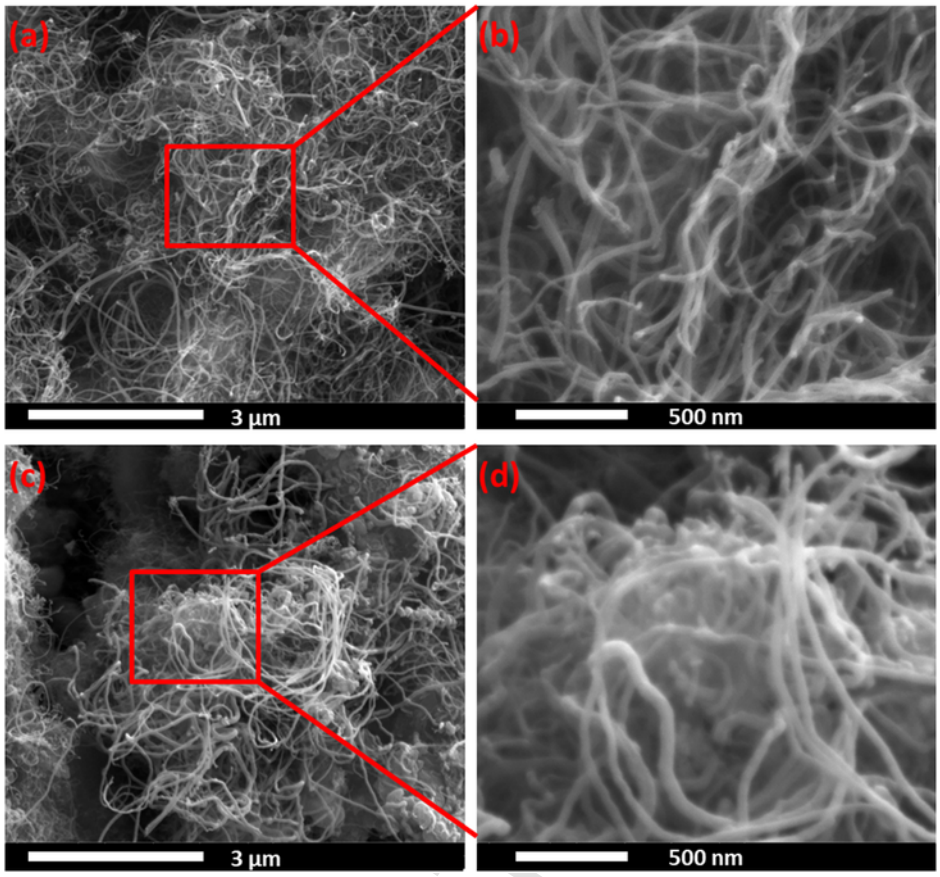

Fig. 4. ESEM images of CNTs synthesized via flux of C_2H_4 (a–b) and of C_2H_4 with H_2 (c–d) on siliceous breccia powder at 750 °C. Panels c and d are the magnifications of the regions highlighted with the red squares. (For interpretation of the references to colour in this figure legend, the reader is referred to the web version of this article.)

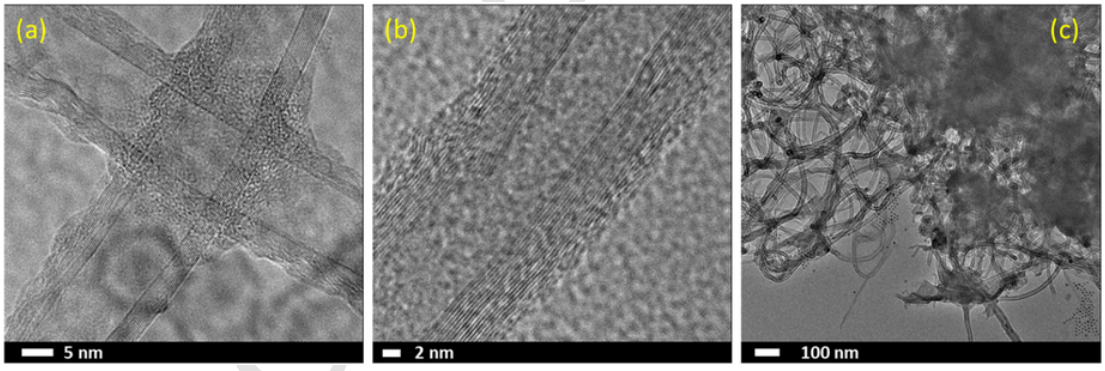

Fig. 5. TEM images of the CNTs on the siliceous breccia powder using CVD. (a–b) TEM of CNTs; (c) CNTs with amorphous carbon and catalyst nanoparticles agglomeration.

2. Experimental section

2.1. Materials

Siliceous Breccia is a rock originated from hydrofracturing of ultramafic rocks, mainly composed of quartz which contains fragments and fissure fillings of serpentine and clay minerals [32]. In the present work, SB was used, obtained from drill core extracted in a mine in New Caledonia. The sample was taken in the frame of the EU H2020 SOLSA project (Grant number 689868, www.solsa-mining.eu). The starting material for the synthesis was a microcrystalline powder with a particle size less than 80 µm.

2.2. Catalyst preparation and hydrocarbon decomposition

CNTs were synthesized on siliceous breccia powder via catalytic CVD using a three-zone atmospheric-pressure furnace. The furnace was equipped with a fused-silica tube having an internal diameter of 22 mm. Given that siliceous breccia contains similar catalytic elements to the natural laterite, the experimental parameters, i.e., temperature, gas flows, and duration of the reaction, were set according to the parameters that optimized synthesis of CNTs using natural laterite ore powders - please refer to reference [24] for a discussion of the process parameters. The temperatures of the three zones were kept fixed and were monitored using built-in furnace thermocouples. The pristine SB powder was placed in the ceramic boat placed into the furnace outside

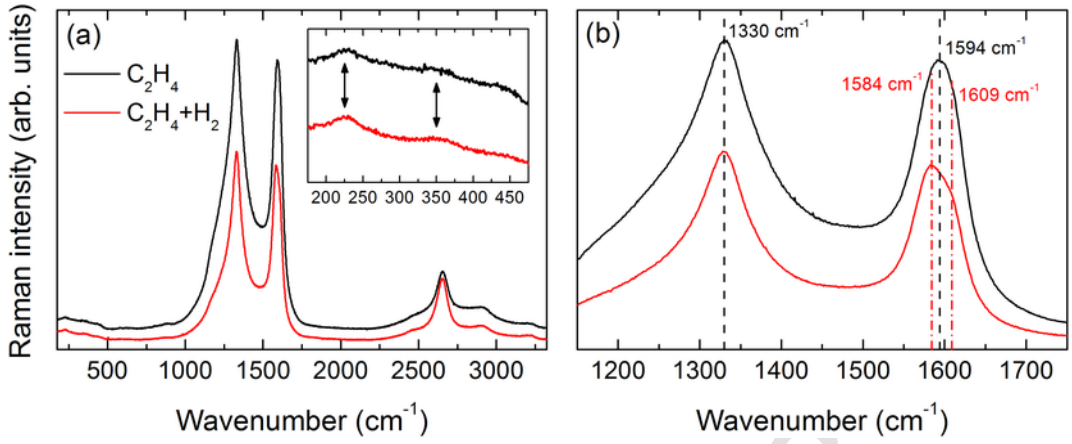

Fig. 6. (a) Typical experimental Raman spectra on CNTs synthesized as described in the text; the details of the low-wavenumber region are shown in the inset where the positions of the RBM are marked with black arrows. (b) Partial spectra in the graphitic modes region showing the profile details of the D and G bands. Colors are as in the legend. (For interpretation of the references to colour in this figure, the reader is referred to the web version of this article.)

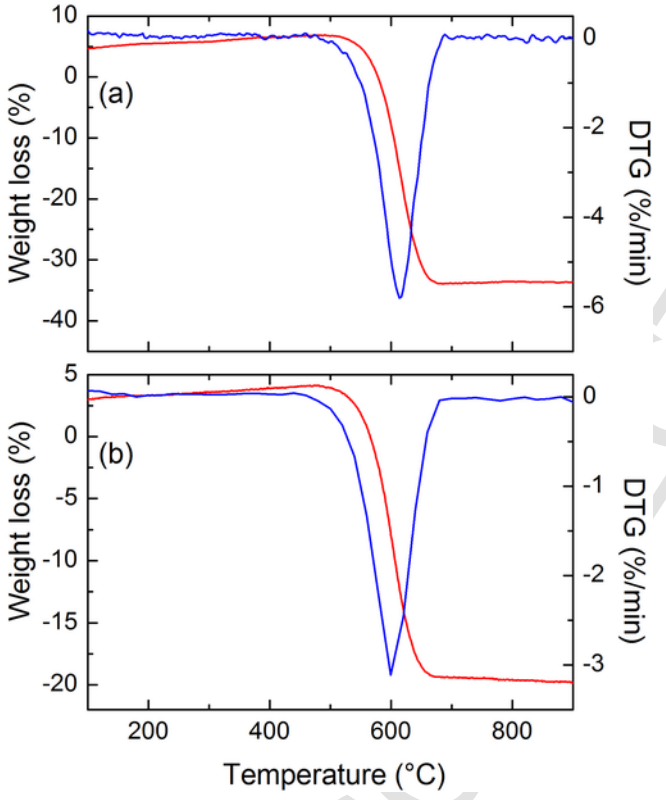

Fig. 7. Thermogravimetric curves of the CNTs synthesized under undiluted C_2H_4 (a) and under C_2H_4 with H_2 (b). Red lines are the TGA (left axis) and the blue ones are the DTG (right axis). (For interpretation of the references to colour in this figure legend, the reader is referred to the web version of this article.)

its hot zone and was first purged at room temperature for 30 min under an inert atmosphere of Ar gas (99.9999%, Gas Technologies) with 100 sccm flow. In order to synthesize CNTs, the sample was then moved into the hot zone of the furnace using the "fast heat" technique, which we described in other publications [33–35], and was reduced in situ with Ar/H_2 gases at 100/400 sccm at 700 °C for 15 min. After the reduction process, we continued flowing Ar gas while increasing the hot zone temperature to the growth temperature (750 °C) and keeping the catalyst in the hot zone. Once the growth temperature was attained, the Ar gas flow was closed and undiluted C_2H_4 (100 sccm) and C_2H_4/H_2 (100/30) was introduced into the furnace for 30 min. We introduced the flux for a lesser time duration than that reported for CNTs and nanofibers production using natural lava as catalyst, for which the flux flow was 2 h [17]. After the reaction, the quartz tube was shifted out of the furnace and was cooled to room temperature under a 100 sccm flow of Ar gas. Gas flows were maintained using an electronic mass flow unit, equipped with digital mass flow controllers.

2.3. Characterization techniques

The starting materials, as well as the synthesized carbon nanomaterials, were characterized using different techniques. The crystalline structure of the pristine powders was determined using X-ray diffraction (XRD). Data were obtained using a Thermo ARL X'TRA powder diffractometer, operating in Bragg-Brentano geometry. The instrument is equipped with a Cu-anode X-ray source (K_α, $\lambda = 1.5418$ Å) and a Peltier Si(Li) cooled solid state detector. Samples were scanned from 15° to 75° (2θ) with an angular step of 0.025°.

The morphology of the synthesized CNTs was observed using an FEI Quanta FEG 250 environmental scanning electron microscope (ESEM), under an operating voltage of 15 kV.

Both high-resolution surface morphology and intimate structure of the synthesized CNTs were investigated using a JEOL, model JEM 1400, transmission electron microscope (TEM), operated at 18 keV.

A careful vibrational spectroscopy analysis of the pristine powder and of the synthesized carbon nanomaterials was carried out using an Horiba Jobin-Yvon LabRam HR800 micro-Raman spectrometer. This system was equipped with a He-Ne laser as an excitation source ($\lambda_{exc} = 632.8$ nm) and a notch filter for the rejection of the Rayleigh line. Raman spectra were carried out in backscattering geometry over the Stokes-shifted region, while the irradiation power at the surface of the sample was kept below 2 mW. The laser beam was focused over the selected sample region, through a long working distance 80× objective, having a numerical aperture, N.A. = 0.75 and giving a spot size of about 1 μm onto the sample surface. The scattered radiation was dispersed by a 600 lines/mm diffraction grating and detected at the spectrograph output by a red-extended multichannel detector, a CCD with 1024 × 256 pixels, cooled by liquid nitrogen. The spectral resolution was about 1 cm^{-1}/pixel over the spectral range of interest.

The thermal analysis of the synthesized carbon nanomaterials was carried by means of an STA 449C Jupiter® analyzer (Netzsch-Gerätebau GmbH, Selb, Germany) in the temperature range between 20 °C and 1000 °C at a heating rate of 10 °C min^{-1} under the constant air flux of 50 sccm min^{-1}.

3. Results and discussions

3.1. Siliceous breccia as catalyst source

The ESEM image of a typical grain of the siliceous breccia powder and a detail of it observed under higher magnification, are shown in Fig. 1.

The EDX microanalysis of the starting material reveals the presence of O, Si, Fe and Mg, each one occurring in different amounts (see Table 1).

Fig. 2 shows a typical experimental XRD pattern acquired on the SB powder. According to Ref. [36, 37], the observed pattern corresponds to that of SiO_2, α-quartz. No further phase was detected by XRD.

Fig. 3 shows two typical experimental Raman spectra measured in the starting powder within a systematic micro-Raman characterization study. The spectrum reported in Fig. 3a consists of a set of Raman bands peaked at about 124, 197, 262, 354, 394, 464, 694, 805, 1080, and 1160 cm^{-1}. They are the vibrational fingerprints of α-quartz [38,39]. The strongest band, at around 464 cm^{-1}, corresponds to the A_1 total symmetric vibration. The spectrum shown in Fig. 3b displays a series of bands, the main of which, centered at about 243, 297, 385, 550, and 685 cm^{-1}, are typical signature of goethite, γ-FeOOH. In fact, the shape of the overall spectrum, the peak positions and the relative intensity of the component bands correspond to the reported ones in the literature for goethite [40,41]. The systematic Raman investigation of the material shows that quartz is the main phase, while goethite occurs in form of micro-inclusions, embedded within the quartz.

In summary, the results of the different characterizations indicate that the pristine SB powder is formed by SiO_2 α-quartz and iron oxide-hydroxides, mainly goethite, which occurs in form of micro-inclusions, incorporated into the quartz matrix. The amount of Fe determined by EDX is about 0.39 wt%. Iron is contained in sub-micrometric or micrometric inclusions randomly distributed among silicate regions and acts as a catalyst, thus making this material suitable for CNT growth.

3.2. Synthesized carbon nanotubes

The morphology of the carbon nanostructures grown by CVD over siliceous breccia powders was observed with ESEM. Fig. 4 represents the ESEM images, obtained with two different magnifications of the materials obtained using undiluted C_2H_4 (panels a and b) and with C_2H_4 diluted with 30 sccm of H_2 (panels c and d). The images clearly show the presence of nanotube-like structures, most likely multiwall carbon nanotubes (MWCNT), arranged in bundle formations; CNTs are observed all over the catalyst surface although some regions contain dense agglomerations of CNTs while some other do not show any CNT presence. This inhomogeneous growth may be caused by the non-uniform distribution of iron oxide-hydroxide particles on the SB surface. The growth can be due to the microinclusions of iron oxyhydroxide, as a source of Fe particles in the catalysts, which have been already identified as nucleation centers for CNT growth [19]. Moreover, the addition of H_2 to C_2H_4 stream changes the ratio of carbon to H_2 and affects the growth of carbon nanostructures, which results in the growth of CNTs with enhanced length and diameter. We obtained non-distorted CNTs without any purification as suggested in the case of non-modified natural zeolite [14]. We also observed that the nanotubes have open ends when H_2 was flown with C_2H_4 (see Fig. 4d). Similar findings were reported by other researchers, too [27,42]. The plausible rationale behind this process is the removal of the amorphous carbon under H_2 treatment at high temperature [42].

Alongside the external surface morphology of MWCNTs portrayed by ESEM, we have also exploited TEM approach in the aim to get more insights about the intimate structure of these carbon nanostructures. In fact; while the overall arrangement of MWCNTs at the micron scale is generally evaluated from ESEM analysis, TEM investigation should be mandatory implemented for the CNTs diameter evaluation [43].

Using TEM, we characterized the structure of the CNTs over the metal catalyst particles derived from siliceous breccia powder at 750 °C from the decomposition of C_2H_4 with H_2. It is widely accepted that the CNTs diameter can be determined by directly measuring the distance between two dark lines associated with CNTs contour in a TEM image [44,45]. Typical high-resolution TEM images of CNTs are reported in Fig. 5 (panels a and b), they show CNT diameters approximately in the range of 25–35 nm with some 15 to 20 walls. We can clearly see the walls of the CNTs, which indicate a high level of crystallinity as compared to that of the magnesite sample [19] where SWCNTs with diameters of about 1.0–1.8 nm were obtained along with tubes bundles in the range of 5–20 nm. Further, most CNTs showed several bulk black areas caused by the amorphous carbon and catalyst agglomeration as well as terminated with graphitic carbon (Fig. 5c), similarly to what we previously reported in our study on natural laterite used as catalyst source [24]. The observed phenomenology could follow the process that reported by [43] that, after the opening of the CNT, it begins to fill with amorphous carbon fragments (see Fig. 5c). This process was attributed to the peeling of inner layers and amorphous carbon fragments along with the catalyst particles draw passively into the CNTs structure [43,46].

The full experimental Raman spectra of the synthesized MWCNTs are shown in Fig. 6a, either for C_2H_4 (black line) and C_2H_4 with H_2 (red line). In the low-wavenumber region, at about 225 cm^{-1} and at about 350 cm^{-1}, both spectra show the presence of weak bands due to Radial Breathing Modes (RBM), which are characteristic features of MWCNTs [47]. The intensities of these RBM turn out to be a little stronger in samples obtained by flowing H_2 together with C_2H_4 thus confirming the effect of the H_2 in enhancing the growth of CNTs. Besides the low-wavenumber region, both spectra show the two characteristic features of highly disordered graphitic forms of carbon, namely the D band, centered at about 1330 cm^{-1} and a second band, nearby 1590 cm^{-1}, known as the G band. The related Raman spectra, as-recorded on the two samples, are shown in Fig. 6b. The D band peaked at 1330 cm^{-1} is due to some structural disorder of the graphitic component, i.e. of the sp^2 carbon domains [48,49]. Conversely, the G band is associated with the in-plane carbon-carbon stretching vibrations in two adjacent graphitic layers, i.e. to an E_{2g} symmetry mode of the graphite unit cell [48,49]. The G band is peaked at 1594 cm^{-1} in the spectrum of sample deposited under C_2H_4 flow, while in the sample deposited with H_2 it results peaked at about 1584 cm^{-1}. Moreover, in this sample, a third band occurs at about 1609 cm^{-1}, as a shoulder of the G band. This band, known as the D' band, can be related to the presence of defects outside the graphitic layers [50]. Moreover, for both samples, together with the D and G bands, some second-order Raman bands are also observed: in particular, the 2D band, overtone of the D band, at 2654 cm^{-1}, the combination of D and G bands, referred as D + G band, at 2922 cm^{-1}, and the overtone of the G band at about 3200 cm^{-1}, are clearly visible. The 2D band is sensitive to the stacking order of the graphitic sheets and its intensity can be therefore correlated with the CNTs structural arrangement. Generally, the I_D/I_G ratio is used to evaluate the structural defects in the non-crystalline carbon materials. In our case, I_D/I_G ratio in the Raman spectra does not show any significant change and in both the spectra it was found to be close to 1. However, DiLeo et al. [51] has proposed that defects would reduce the double resonance process that results in the decreasing of the 2D band intensity, thus making the I_{2D}/I_G ratio a better indicator of crystallinity in MWNTs. Since the 2D band turns out relatively more intense for the CNTs synthesized under H_2 flux (where $I_{2D}/I_G = 0.39$) than that of undiluted C_2H_4 flow (where $I_{2D}/I_G = 0.27$) it is plausible assume that

the intensity increase reflects a more ordered sample structure (i.e., less impurities content).

TEM and micro Raman were employed for purity evaluation of CNTs and the presence of amorphous carbon. It can be clearly observed from the TEM images that most CNTs showed several bulk black areas caused by the amorphous carbon and catalyst agglomeration at the terminated CNTs ends. Further, we would like to emphasize that the spot diameter of the focused laser beam, used for micro-Raman measurements, is about 1 μm, so the irradiated sample region contains a lot of graphitic carbon nanostructures, as evidenced by the TEM images.

In order to investigate the oxidation stability and carbon yield of the final products we have exploietd the thermal gravimetric analysis. TGA gives us the measure the non-carbonaceous impurities in a sample by monitoring the weight decrease of samples during combustion in air. Fig. 7 shows the thermal gravimetric analysis (TGA) and corresponding differential thermal gravimetry (DTG) obtained under undiluted C_2H_4 (panel a) and under C_2H_4 with H_2 (panel b). Red curves represent the carbon yields obtained over catalysts with one step of carbon oxidation. The peak near 600 °C is attributed to the oxidation of CNTs [24,52]. The weight loss is mainly due to the combustion of carbon and is about 43% and 27% for CNT obtained without and with H_2 respectively. The carbon yield obtained from the SB powder is low in comparison to that of about natural laterite, where the carbon yield obtained was about 70% [24]. This may be because of the lower Fe content present in SB powder. TGA results confirm the thermal and oxidation stability of the CNTs. However, the TGA results suggest a different degree of CNTs purity with respect to the expected one on the basis of TEM images. This may occur because the density of SiO_2 is much higher than that of carbon materials. Moreover, the evaluation of the weight ratio of the impurities versus the carbon content is difficult, especially by TEM image analysis. Nevertheless, the two methods complement each other. Finally, we believe that a more accurate evaluation of CNTs purity can be obtained by combining the results of the Raman, TEM, and TGA investigations.

4. Conclusions

MWCNTs with different diameters were synthesized over a siliceous breccia powder catalyst by CVD of C_2H_4 with and without H_2. The combination of ESEM, TEM, and micro-Raman spectroscopy provide a clear structural and vibrational picture the synthesized material leading to highly graphitized CNTs. The TGA profile shows an oxidation peak at about 600 °C thus confirming the thermal and oxidation stability of the CNTs. Our experiments show that the amounts of Fe in the natural siliceous breccia could have a positive role in the growth of CNTs. However, the random 'spaghetti' orientations of the CNTs indicate that the amount of active catalysts in the powder is too low to lead to the growth of vertically aligned CNT carpets. In conclusion, this work presents the use of a new natural catalyst source for the growth of CNTs using CVD during which the naturally contained Fe serves as the active phase and the layered oxides are the support. This technique offers several advantages such as easy availability, low cost, easy to produce CNTs via a simple route. Fabrication of CNTs on naturally occurring minerals without synthetically prepared catalyst could pave the way for further exploitation of the superior properties of tailored nanostructured carbon for large-scale applications.

Acknowledgments

The authors would like to thank: F. Trotet, M. Kadar and K. Devaux (ERAMET-SLN, New Caledonia), A. Salaün and C. Rodriguez (ERAMET) for providing the siliceous breccia powders. This work has been developed within SOLSA project (www.solsa-mining.eu), funded by the European Commission through H2020 programme (grant number SC5-11d-689868).

References

[1] P.M. Ajayan, Nanotubes from carbon, Chem. Rev. 99 (1999) 1787–1799.
[2] M.S. Dresselhaus, G. Dresselhaus, P.C. Eklund, Science of Fullerenes and Carbon Nanotubes, Academic Press, New York, 1996.
[3] S.J. Tans, A.R. Verschueren, C. Dekker, Room-temperature transistor based on a single carbon nanotube, Nature 393 (1998) 49–52.
[4] P.G. Collins, P. Avouris, Nanotubes for electronics, Sci. Am. 283 (2000) 38–45.
[5] S.J. Tans, M.H. Devoret, H. Dai, A. Thess, R.E. Smalley, L.J. Geerlings, C. Dekker, Individual single-wall carbon nanotubes as quantum wires, Nature 386 (1997) 474–477.
[6] P. Calvert, Nanotube composites: a recipe of strength, Nature 399 (1999) 210–211.
[7] H.D. Wagner, O. Lourie, Y. Feldman, R. Tenne, Stress-induced fragmentation of multiwall carbon nanotubes in a polymer matrix, Appl. Phys. Lett. 72 (1998) 188–190.
[8] H.J. Dai, J.H. Hafner, A.G. Rinzler, D.T. Colbert, R.E. Smalley, Nanotubes as nanoprobes in scanning probe microscopy, Nature 384 (1996) 147–150.
[9] A.C. Dillon, K.M. Jones, T.A. Bekkedahl, C.H. Kiang, D.S. Bethune, M.J. Heben, Storage of hydrogen in single-walled carbon, Nature 386 (1997) 377–379.
[10] C. Öncel, Y. Yürüm, Carbon nanotube synthesis via the catalytic CVD method: a review on the effect of reaction parameters, Fullerenes, Nanotubes and Carbon Nanostructures 14 (2006) 17–37.
[11] G.D. Nessim, Properties, synthesis, and growth mechanisms of carbon nanotubes with special focus on thermal chemical vapor deposition, Nanoscale 2 (2010) 1306–1323.
[12] M. Kumar, Y. Ando, Chemical vapor deposition of carbon nanotubes: a review on growth mechanism and mass production, J. of Nanosci. and Nanotech. 10 (2010) 3739–3758.
[13] D. Gournis, M.A. Karakassides, T. Bakas, N. Boukos, D. Petridis, Catalytic synthesis of carbon nanotubes on clay minerals, Carbon 40 (2002) 2641–2646.
[14] M. Kadlečíková, J. Breza, K. Jesenák, K. Pastorková, V. Luptáková, M. Kolmačka, A. Vojačková, M. Michalkac, I. Vávra, Z. Križanová, The growth of carbon nanotubes on montmorillonite and zeolite (clinoptilolite), Appl. Surf. Sci. 254 (2008) 5073–5079.
[15] K. Pastorková, K. Jesenák, M. Kadlečíková, J. Breza, M. Kolmačka, M. Čaplovičová, F. Lazišťan, M. Michalka, The growth of multi-walled carbon nanotubes on natural clay minerals (kaolinite, nontronite and sepiolite), Appl. Surf. Sci. 258 (2012) 2661-266.
[16] D.S. Su, A. Rinaldi, W. Frandsen, G. Weinberg, Nanocarbons: efficient synthesis using natural lava as supported catalyst, phys. stat. sol. (b) 244 (2007) 3916–3919.
[17] D.S. Su, X.W. Chen, Natural lavas as catalysts for efficient production of carbon nanotubes and nanofibers, Angew. Chem. Int. Ed. 46 (2007) 1823–1824.
[18] D.S. Su, The use of natural materials in nanocarbon synthesis, ChemSusChem 2 (2009) 1009–1020.
[19] S. Kawasaki, M. Shinoda, T. Shimada, F. Okino, H. Touhara, Single-walled carbon nanotubes grown on natural minerals, Carbon 44 (2006) 2139–2144.
[20] J.B. Nagy, G. Bister, A. Fonseca, D. Méhn, Z. Kónya, I. Kiricsi, Z.E. Horváth, L.P. Biró, On the growth mechanism of single-walled carbon nanotubes by catalytic carbon vapor deposition on supported metal catalysts, J. Nanosci. Nanotech. 4 (2004) 326–345.
[21] A. Kukovecz, Z. Konya, N. Nagaraju, I. Willems, A. Tamasi, A. Fonseca, J.B. Nagy, I. Kiricsi, Catalytic synthesis of carbon nanotubes over Co, Fe and Ni containing conventional and sol gel silica aluminas, Phys. Chem. Chem. Phys. 2 (2000) 3071–3076.
[22] C.J. Lee, J. Park, J.A. Yu, Catalyst effect on carbon nanotubes synthesized by thermal chemical vapor deposition, Chem. Phys. Lett. 360 (2002) 250–255.
[23] S. Inoue, K. Nomura, Y. Matsumura, Influence of catalyst supporters on catalyst nanoparticles in synthesis of single-walled carbon nanotubes, Microelectron. J. 40 (2009) 692–696.
[24] A. Kumar, Y. Kostikov, B. Orberger, G.D. Nessim, G. Mariotto, Natural laterite as a catalyst source for the growth of carbon nanotubes and nanospheres, ACS Applied Nano Materials 1 (2018) 6046–6054.
[25] Y.M. Manawi, Ihsanullah, A. Samara, T. Al-Ansari, M.A. Atieh, A review of carbon nanomaterials' synthesis via the chemical vapor deposition (CVD) method, Materials 11 (2018) 822–3758.
[26] A. Magrez, J.W. Seo, R. Smajda, M. Mionić, L. Forró, Catalytic CVD synthesis of carbon nanotubes: towards high yield and low temperature growth, Materials 3 (2010) 4871–4891.
[27] T.C. Cheng, Effect of nitrogen and hydrogen on the growth of multiwall carbon nanotubes on flexible carbon cloth using thermal chemical vapor deposition, Mater. Chem. Phys. 136 (2012) 140–145.
[28] G. Zhang, D. Mann, L. Zhang, A. Javey, Y. Li, E. Yenilmez, Q. Wang, J.P. McVittie, Y. Nishi, J. Gibbons, Ultra-high-yield growth of vertical single-walled carbon nanotubes: hidden roles of hydrogen and oxygen, Proc. Natl. Acad. Sci. U. S. A. 102 (2005) 16141–16145.
[29] Y. Li, K. Ji, Y. Duan, G. Meng, Z. Dai, Effect of hydrogen concentration on the growth of carbon nanotube arrays for gecko-inspired adhesive applications, Coatings 7 (2017) 221–232.
[30] I. Pełech, U. Narkiewicz, Studies of hydrogen interaction with carbon deposit containing carbon nanotubes, J. of Non-Cryst. Sol. 355 (2009) 1370–1375.
[31] https://en.wikipedia.org/wiki/Breccia.
[32] M. Secchi, M. Zanatta, E. Borovin, M. Bortolotti, A. Kumar, M. Giarola, A. Sanson, B. Orberger, N. Daldosso, S. Gialanella, G. Mariotto, M. Montagna, L. Lutterotti,

[33] G.D. Nessim, M. Seita, K.P. O'Brien, A.J. Hart, R.K. Bonaparte, R.R. Mitchell, C.V. Thompson, Low temperature synthesis of vertically aligned carbon nanotubes with electrical contact to metallic substrates enabled by thermal decomposition of the carbon feedstock, Nano Lett. 9 (2009) 3398–3405.

[34] G.D. Nessim, A. Al-Obeidi, H. Grisaru, E.S. Polsen, C.R. Oliver, T. Zimrin, A.J. Hart, D. Aurbach, C.V. Thompson, Synthesis of tall carpets of vertically aligned carbon nanotubes by in situ generation of water vapor through preheating of added oxygen, Carbon 50 (2012) 4002–4009.

[35] E. Teblum, A. Itzhak, E. Shawat-Avraham, M. Muallem, R. Yemini, G.D. Nessim, Differential preheating of hydrocarbon decomposition and water vapor formation shows that single ring aromatic hydrocarbons enhance vertically aligned carbon nanotubes growth, Carbon 109 (2016) 727–736.

[36] http://rruff.info/quartz/source/asc/R100134.

[37] M.C. Morris, H.F. McMurdie, E.H. Evans, B. Paretzkin, H.S. Parker, N.C. Panagiotopoulos, C.R. Hubbard, Standard X-ray Diffraction Powder Patterns Section 18-Data for 58 Substances, National Bureau of Standards, Washington, DC, USA, 198161.

[38] J.F. Scott, S.P.S. Porto, Longitudinal and transverse optical lattice vibrations in quartz, Phys. Rev. 161 (1967) 903–910.

[39] K.J. Kingma, R.J. Hemley, Raman spectroscopic study of microcrystalline silica, Am. Mineral. 79 (1994) 269–273.

[40] D. Faria, S. Silva, M. Oliveira, Raman microspectroscopy of some iron oxides and oxyhydroxides, J. Raman Spectrosc. 28 (1997) 873–878.

[41] M.A. Legodi, D. Waal, The preparation of magnetite, goethite, hematite and maghemite of pigment quality from mill scale iron waste, Dyes Pigments 74 (2007) 161–168.

[42] S.R.C. Vivekchand, A. Govindaraj, Md. Motin Seikh, C.N.R. Rao, New method of purification of carbon nanotubes based on hydrogen treatment, J. Phys. Chem. B 108 (2004) 6935–6937.

[43] J.H. Lehman, M. Terrones, E. Mansfield, K.E. Hurst, V. Meunier, Evaluating the characteristics of multiwall carbon nanotubes, CARBON 49 (2011) 2581–2602.

[44] C. Branca, F. Frusteri, V. Magazù, A. Mangione, Characterization of carbon nanotubes by TEM and infrared spectroscopy, J. Phys. Chem. B 2004, 108, 3469–3473.

[45] C. Qin, L.M. Peng, Measurement accuracy of the diameter of a carbon nanotube from TEM images, Phys. Rev. B 65 (2002) 155431–155437.

[46] P.M. Ajayan, T.W. Ebbesen, T. Ichihashi, S. Iijima, K. Tanigaki, H. Hiura, Opening carbon nanotubes with oxygen and implications for filling, Nature 362 (1993) 522–525.

[47] X. Zhao, Y. Ando, L.C. Qin, H. Kataura, Y. Maniwa, R. Saito, Characteristic Raman spectra of multiwalled carbon nanotubes, Physica B 323 (2002) 265–266.

[48] F. Tuinstra, J.L. Koenig, Raman spectrum of graphite, J. Chem. Phys. 53 (1970) 1126–1130.

[49] R.J. Nemanich, S.A. Solin, First- and second-order Raman scattering from finite-size crystals of graphite, Phys. Rev. B 20 (1979) 392–401.

[50] A.C. Ferrari, J. Robertson, Interpretation of Raman spectra of disordered and amorphous carbon, Phys. Rev. B 61 (2000) 14095–14107.

[51] R.A. DiLeo, B.J. Landi, R.P. Raffaelle, Purity assessment of multiwalled carbon nanotubes by Raman spectroscopy. J. Appl. Phys. 101 (2007) 064307-5.

[52] H.S. Yang, L. Zhang, X.H. Dong, W.M. Zhu, J. Zhu, B.J. Nelson, X.B. Zhang, Precise control of the number of walls formed during carbon nanotube growth using chemical vapor deposition, Nanotechnology 23 (2012) 065604–065609.